A STUDY ON CONTINUOUS MAX-FLOW AND MIN-CUT APPROACHES

JING YUAN*, EGIL BAE†, XUE-CHENG TAI‡, AND YURI BOYKOV§

Abstract. We propose and investigate novel max-flow models in the spatially continuous setting, with or without supervised constraints, under a comparative study of graph based max-flow / min-cut. We show that the continuous max-flow models correspond to their respective continuous min-cut models as primal and dual problems, and the continuous min-cut formulation without supervision constraints regards the well-known Chan-Esedoglu-Nikolova model [15] as a special case. In this respect, basic conceptions and terminologies applied by discrete max-flow / min-cut are revisited under a new variational perspective. We prove that the associated nonconvex partitioning problems, unsupervised or supervised, can be solved globally and exactly via the proposed convex continuous max-flow and min-cut models. Moreover, we derive novel fast max-flow based algorithms whose convergence can be guaranteed by standard optimization theories. Experiments on image segmentation, both unsupervised and supervised, show that our continuous max-flow based algorithms outperform previous approaches in terms of efficiency and accuracy.

Key words. image processing and segmentation, continuous max-flow / min-cut, optimization

AMS subject classifications. ...

1. Introduction. Many applications of image processing and computer vision can be modeled in the form of energy minimization through Markov Random Fields (MRF) and solved by means of min-cut and max-flow, see [39, 38] for a good reference. A long list of successful examples includes image segmentation [10, 2, 5], stereo [31, 32], 3D reconstruction and shape-fitting[44, 36, 37], image synthesis and photomontage [34, 1], etc. The discrete energy minimization problems are often tackled by searching for the minimal cut over an appropriately constructed graph, which can be efficiently computed by maximization of corresponding flows by the classical theorem of min-cut and max-flow [19, 16]. There has been a vast amount of research on this topic during the last years [8, 10]. Other discrete optimization methods include message passing [45, 29] and linear programming [33] etc. One main drawback of such graph-based approaches is the grid bias. The interaction potential penalizes some spatial directions more than other, which leads to visible artifacts in computational results. Reducing such metrication errors can be done by considering more neighboring nodes [9, 28] or high-order interaction potentials [27, 25]. However, this either results in a heavy memory load and high computation cost or amounts to a more complex algorithmic scheme, e.g. QPBO [7, 30].

Recent studies [15] showed that formulating min-cut in the spatially continuous setting properly avoids metrication bias and leads to fast and global numerical solvers through convex optimization [11]. G. Strang [41, 42] was the first to study max-flow and min-cut problems over a continuous domain. Related studies include [2, 3], where Appleton et al proposed an edge-based continuous minimal surface approach to segmenting 2D and 3D objects. Chan et al [15] considered image segmentation with two regions in the form

$$\min_{S} \int_{\Omega \setminus S} C_s(x)\, dx + \int_{S} C_t(x)\, dx + \alpha \left|\partial S\right| . \tag{1.1}$$

*Jing Yuan, Computer Science Department, Middlesex College, University of Western Ontarion, London Ontario, Canada N6A 5B7 (cn.yuanjing@gmail.com)

†Egil Bae, Department of Mathematics, University of Bergen, Norway. (egil.bae@math.uib.no)

‡Xue-Cheng Tai, Division of Mathematical Sciences, School of Physical and Mathematical Sciences, Nanyang Technological University, Singapore and Department of Mathematics, University of Bergen, Norway. (tai@mi.uib.no)

§Yuri Boykov, Computer Science Department, Middlesex College, University of Western Ontarion, London Ontario, Canada N6A 5B7 (yuri@csd.uwo.ca)

By means of relaxing the characteristic function $\lambda(x) \in \{0,1\}$ of S to $\lambda(x) \in [0,1]$, Chan et al proved that the binary-constrained nonconvex formulation (1.1) can be globally solved by the convex minimization problem

$$\min_{\lambda(x)\in[0,1]} \int_\Omega (1-\lambda(x))C_s(x)\,dx \;+\; \int_\Omega \lambda(x)C_t(x)\,dx \;+\; \alpha \int_\Omega |\nabla\lambda(x)|\;dx\,. \qquad (1.2)$$

More specifically, solving (1.2) leads to a sequence of global binary optimums through thresholds of its optimum $\lambda^*(x) \in [0,1]$ by any value $t \in (0,1]$. In consequence, it gives rise to a set of global binary solutions to the original nonconvex partition problem (1.1), not just one which is the case for graph-cuts. In this regard, (1.2) is actually known as the *continuous min-cut model*. We will revisit this model in Sec. 2. Recently, Chan's approach was extended to more than two regions in [40, 35, 4], i.e. the continuous Potts model, although no simple thresholding scheme as above has been discovered for these relaxed models.

However, in contrast to the duality between discrete max-flow and min-cut models [19] where efficient min-cut algorithms are designed in a max-flow fashion [16], max-flow models over a continuous image domain, as the dual formulation of (1.2), is still lost in recent developments. For minimization problems involving total variation like the ROF model [13], where the primal variable is unconstrained, dual formulations are also known and has been used to design fast algorithms. However, if constraints like $u \in [0,1]$ are introduced, the dual formulation changes completely, as we will see. To tackle such constraints in research so far, algorithms which are designed for unconstrained total variation have been applied. They are simply modified such that the primal variable is forced to the feasible set every iteration, either by projections or by adding forcing terms [15, 11, 22]. This is in contrast to graph cuts where the min-cut problem can be restated as a max-flow problem in an elegant way and helps to significantly accelerate the algorithms, e.g. the Ford-Fulkerson algorithm [16], push-relabel algorithm [21], Dinitz blocking flow algorithm [17] etc. Recently Bae et al [4] studied the dual formulation of the continuous Potts problem with multiple labels, but not in the manner of maximizing flows. This motivates our studies in this work. Moreover, we will also investigate the min-cut problem with priori supervision constraints by adapting its supervised information into the corresponding max-flow structures.

1.1. Contributions. We contribute this paper to propose and study new continuous max-flow formulations, which are in analogy with the discrete graph based max-flow models. In other words, we will explore and solve continuous min-cut problems with or without supervision constraints by the means of the proposed continuous max-flow models. This is in contrast to previous works.

We summarize our main contributions in this work as follows:

First, we propose novel continuous max-flow models, which provide new equivalent representations of their respective continuous min-cut problems, unsupervised (1.2) or supervised (4.12), in terms of primal and dual.

Second, we revisit and give explanations of fundamental conceptions used in graph cuts, e.g. 'saturated' / 'unsaturated' and 'cuts', through a new variational perspective which also provides a new viewpoint to understand the classical max-flow / min-cut algorithms. Via the equivalent max-flow formulation, we prove that the nonconvex image segmentation problems, unsupervised (1.1) and supervised (4.1), can be solved exactly and globally in a convex relaxation way.

Third, for the continuous min-cut model under supervised constraints, the proposed continuous max-flow formulation encodes such user-input constraints implicitly, which does not require to change flow capacities artificially as is done previously. Meanwhile, the complexities of the new supervised max-flow and min-cut models are the same as the unsupervised

ones.

Finally, new and fast max-flow based algorithms are proposed, which splits the optimization problem into simple subproblems over independent flow variables, where the labeling function $\lambda(x)$ works as a multiplier and can be simply updated at each iteration. Their convergence can be easily validated by classical optimization theories. Experiments show our continuous max-flow algorithms significantly outperform previous continuous min-cut methods in terms of efficiency, e.g. [11], and graph based methods in terms of accuracy. This work extends [46] with detailed proofs and more extensive experimental evaluation.

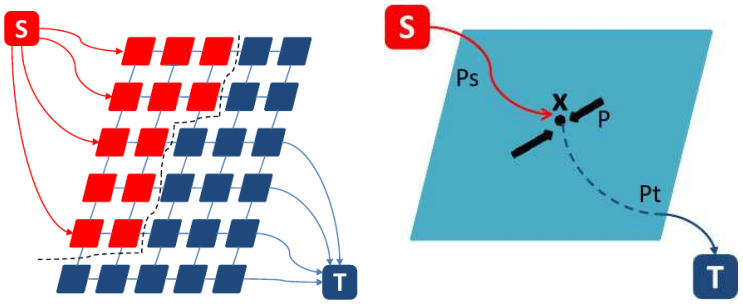

FIG. 2.1. **Settings of Max-Flow and Min-Cut**, *Discrete (left) vs. Continuous (right)*

2. Related Works.

2.1. Revisit of Discrete Max-Flow and Min-Cut. Many optimization problems in image processing and computer vision can be formulated as max-flow/min-cut problems on appropriate graphs, as first observed by Greig et. al. [23]. A graph $\mathcal{G}$ is a pair $(\mathcal{V}, \mathcal{E})$ consisting of a vertex set $\mathcal{V}$ and an edge set $\mathcal{E} \subset \mathcal{V} \times \mathcal{V}$.

The vertex set of commonly-used graphs in image processing and computer vision includes the nodes in a 2-D or 3-D nested grid, together with two terminal vertices, the source s and the sink t, e.g. see the left graph of Fig. 2.1. The edge set is comprised of two types of edges: the spatial edges $e_n = (r, q)$, where $r, q \in \mathcal{V}\backslash\{s, t\}$, stick to the given grid and link two neighbor grid stencils r and q except s and t; the terminal edges or data edges, i.e. $e_s = (s, r)$ or $e_t = (r, t)$, where $r \in \mathcal{V}\backslash\{s, t\}$, link the specified terminal s or t to each grid node p respectively. We assign a cost $C(e)$ to each edge e, which is assumed to be nonnegative i.e. $C(e) \geq 0$. In this work, we consider this type of graphs in the 2-D case mainly for simplicities. Of course, our discussions can be easily extended to the 3-D case.

2.1.1. Min-Cut. Based on the above discrete configuration, the two-partition cut assigns two disjoint partitions to the source s and the sink t respectively, also called *s-t cut*. Obviously, it divides the spatial grid nodes of Ω into two disjoint groups: one relates to the source s and the other one to the sink t, hence segments the given image nodes into two different parts (see the left graph of Fig. 2.1):

$$\mathcal{V} = \mathcal{V}_s \bigcup \mathcal{V}_t\,, \quad \mathcal{V}_s \cap \mathcal{V}_t = \emptyset\,.$$

To each cut, an energy is defined as the sum of the costs $C(e)$ of each edge $e \in \mathcal{E}_{st} \subset \mathcal{E}$, whose end-points belong to two different partitions. Hence the problem of min-cut is to find two partitions of vertices such that the corresponding cut-energy is minimal:

$$\min_{\mathcal{E}_{st} \subset \mathcal{E}} \sum_{e \in \mathcal{E}_{st}} C(e)\,. \tag{2.1}$$

2.1.2. Max-Flow. On the other hand, each edge $e \in \mathcal{E}$ can be viewed as a pipe and the edge cost $C(e)$ can be regarded as the capacity on this pipe, for which the maximal flow is allowed. For such a 'pipe' network, we have the following constraints on flows:

- Capacity of Spatial Flows p: for undirected spatial edges $e_n = (r, q) \in \mathcal{E}$, $r, q \in \mathcal{V}\backslash\{s, t\}$, the spatial flow $p(e_n)$ is constrained by:

$$|p(e_n)| \leq C(e_n)\,; \tag{2.2}$$

  here we use the same flow capacity for both the two directions $r \to q$ and $q \to r$ for simplicities. This corresponds to an anisotropic total-variation term. In fact, discussions on it in the following sections can be easily extended to the case where different flow capacities $C_{r\to q}, C_{q\to r} \geq 0$ are applied in the two flow directions. Assuming $r \to q$ is the positive direction the constraint would be

$$-C_{q\to r} \leq p(e_n) \leq C_{r\to q}\,.$$

- Capacity of Source Flows p_s: for the edge $e_s(v) : s \to v$ linking the terminal s to a node $v \in \mathcal{V}\backslash\{s, t\}$, the source flow $p_s(v)$ is directed from s to v. Its capacity $C_s(v)$ indicates that

$$0 \leq p_s(v) \leq C_s(v)\,; \tag{2.3}$$

- Capacity of Sink Flows p_t: for the edge $e_t(v) : v \to t$ linking a node $v \in \mathcal{V}\backslash\{s, t\}$ to the terminal t, $p_t(v)$ is directed from v to t. Its capacity $C_t(v)$ indicates that

$$0 \leq p_t(v) \leq C_t(v)\,; \tag{2.4}$$

- Conservation of Flows: at each node $v \in \mathcal{V}\backslash\{s, t\}$, incoming flows should be balanced by outgoing flows. In other words, all the flows passing through v, including spatial flows $p(e_n := (v, q))$ where $q \in N(v)$ is in the set of neighboring nodes of v, the source flow $p_s(v)$ and the sink flow $p_t(v)$, should be constrained by

$$\big(\sum_{q\in N(v)} p((q, v))\big) - p_s(v) + p_t(v) = 0\,. \tag{2.5}$$

In this regard, the maximal flow problem is to find the largest amount of flow allowed to pass from the source s to the sink t, i.e.

$$\max_{p_s} \sum_{v\in\mathcal{V}\backslash\{s,t\}} p_s(v)\,, \tag{2.6}$$

subject to the above conditions (2.2), (2.3), (2.4) and (2.5).

It is well known that the max-flow problem (2.6) is equivalent to the min-cut problem (2.1), where the flows are saturated uniformly on the cut edges, i.e. the total flow is bottlenecked by the 'saturated pipes'. By the graph-cut terminologies, when a flow $p(e)$ on the edge $e \in \mathcal{E}$ reaches its corresponding capacity $C(e)$, given by (2.2), (2.3) or (2.4), we call it 'saturated'; otherwise, 'unsaturated'. We will revisit these conceptions under a variational perspective in the following sections.

2.2. Convex Relaxation and Continuous Min-Cut. As in Sec. 1, Chan et al [15] introduced an exact convex relaxation formulation (1.2) to the nonconvex segmentation problem (1.1), which results in a global optimization framework for the well-known active contour/snake model [26, 12] with region priors, e.g. active contour without edges [14]. The

authors applied a comparatively slow PDE-descent scheme in numerics, together with an exact penalty term to enforce the pointwise $[0,1]$ constraints. Experiments in [15] showed the proposed convex relaxation scheme properly avoided the trap of local optimums and was reliable with respect to the given data and initial conditions.

Bresson et al [11] extended Chan et al's work by applying a weighted total-variation term. They also proposed a fast algorithm for (1.2) based on an approximation of (1.2):

$$\min_{\lambda,\mu} \Big\{ \alpha \int_\Omega |\nabla \lambda(x)| \; dx \; + \; \frac{1}{2\theta} \|\lambda - \mu\|^2 \; + \; \int_\Omega \mu(x) \big(C_t(x) - C_s(x) \big) \, dx \; + \; \beta P(\mu) \Big\} \quad (2.7)$$

where $P(\mu) := \int_\Omega \max\{0, 2\,|\mu - 0.5| - 1\}\, dx$ is an exact penalty function which forces $\mu(x)$ to the interval $[0,1]$ pointwise. Clearly, when $\theta > 0$ is chosen small enough, it is expected that $\lambda \simeq \mu$, hence (2.7) solves (1.2) given $\mu(x) \in [0,1]$. To this end, the convex constrained optimization problem (1.2) is approximated by a relatively simple unconstrained optimization formulation (2.7).

In view of (2.7), the authors introduced a fast alternation-descent scheme which includes two inner steps concerning the two variables λ and μ within each outer iteration, i.e. at the k-th iteration,

- fix μ^k and solve

$$\lambda^{k+1} \; := \; \arg\min_{\lambda} \Big\{ \alpha \int_\Omega |\nabla \lambda(x)| \; dx \; + \; \frac{1}{2\theta} \|\lambda(x) - \mu^k(x)\|^2 \Big\}$$

  which can be computed by the standard Chambolle's projection algorithm [13];
- fix λ^{k+1} and solve

$$\mu^{k+1} \; := \; \arg\min_{\mu} \Big\{ \frac{1}{2\theta} \|\mu(x) - \lambda^{k+1}\|^2 + \int_\Omega \mu(x) \big(C_t(x) - C_s(x) \big) \, dx + \beta P(\mu) \Big\}$$

  which can be simply solved in closed form by shrinkage (see Prop. 4 of [11]).

3. Continuous Max-Flow and Min-Cut. In this section, we propose and study the dualitites of max-flow and min-cut in the spatially continuous context.

3.1. Primal Model: Continuous Max-Flow. In the spatially continuous setting, let Ω be a closed spatial 2-D or 3-D domain and s, t be the source and sink terminals, see the right figure of Fig. 2.1. At each point $x \in \Omega$, we denote the usual spatial flow passing x by $p(x)$; the directed source flow from s to x by $p_s(x)$; and the directed sink flow from x to t by $p_t(x)$. Now we consider the counterpart of the discrete max-flow problem (2.6) in this continuous setting, which can be directly formulated in the same manner as stated in Sec. 2.1.

For each $x \in \Omega$ let $p_s(x) \in \mathbb{R}$ denote the flow from the source s to x and $p_t(x) \in \mathbb{R}$ denote the flow from x to the sink t. Define further the vector field $p \;\; : \;\; \Omega \mapsto \mathbb{R}^n$ as the spatial flow within Ω, where n is the dimension of the image domain Ω. In view of the flow constraints (2.2), (2.3), (2.4) and (2.5) in the discrete setting, the flows $p(x), p_s(x), p_t(x)$ are constrained by the capacities $C(x), C_s(x)$ and $C_t(x)$ as follows:

$$|p(x)| \; \leq \; C(x), \quad \forall x \in \Omega; \quad (3.1)$$

$$p_s(x) \; \leq \; C_s(x), \quad \forall x \in \Omega; \quad (3.2)$$

$$p_t(x) \; \leq \; C_t(x), \quad \forall x \in \Omega; \quad (3.3)$$

$$\operatorname{div} p(x) - p_s(x) + p_t(x) \; = \; 0, \quad \text{a.e. } x \in \Omega. \quad (3.4)$$

Here $\operatorname{div} p$ evaluates the total incoming spatial flow locally around x, which is in analogue with the sum operator of (2.5) for discrete settings. The notation a.e. stands for "for almost

every". It means the constraint (3.4) should hold in the integrable, weak sense for every $x \in \Omega$, expect possibly a subset of zero measure.

Here, the constraints on the source flow $p_s(x)$ (3.2) and the sink flow $p_t(x)$ (3.3) are changed in comparison to (2.3) and (2.4). This is because positiveness of the flows $p_s(x)$ and $p_t(x)$ are not needed as they are directed flows and their values indicate how the flow is distributed from s to the point x or from x to t. Likewise, $C_s(x)$ and $C_t(x)$ are also not necessary required to be positive. Therefore, this extends the application of max-flow and min-cut models in the continuous setting.

In analogy with the discrete max-flow problem (2.6), the *continuous max-flow* model can be formulated as

$$\sup_{p_s,p_t,p} \Big\{ P(p_s,p_t,p) \,=\, \int_\Omega p_s(x)\,dx \Big\} \tag{3.5}$$

subject to the constraints (3.1), (3.2), (3.3) and (3.4). In this paper, we also call (3.5) the *primal model* and all flow variables p_s, p_t and p the *primal variables*.

3.2. Primal-Dual Model. By introducing the multiplier $\lambda(x)$, also called the *dual variable*, to the linear equality of flow conservation (3.4), the continuous maximal flow model (3.5) can be formulated as its equivalent *primal-dual model* :

$$\begin{aligned} \sup_{p_s,p_t,p} \inf_{\lambda} \Big\{ E(p_s,p_t,p;\lambda) \,&=\, \int_\Omega p_s(x)\,dx + \int_\Omega \lambda(x)\big(\operatorname{div} p - p_s + p_t\big)\,dx \Big\} \\ \text{s.t.} \quad & p_s(x) \le C_s(x)\,, \quad p_t(x) \le C_t(x)\,, \quad |p(x)| \,\le\, C(x)\,. \end{aligned} \tag{3.6}$$

Rearranging the primal-dual formulation (3.6), we then get

$$\begin{aligned} \sup_{p_s,p_t,p} \inf_{\lambda} \Big\{ E(p_s,p_t,p;\lambda) \,&=\, \int_\Omega \big\{ \big(1-\lambda\big)p_s + \lambda p_t + \lambda \operatorname{div} p \big\}\,dx \Big\} \\ \text{s.t.} \quad & p_s(x) \,\le\, C_s(x)\,, \quad p_t(x) \le C_t(x)\,, \quad |p(x)| \,\le\, C(x)\,. \end{aligned} \tag{3.7}$$

Note that for the primal-dual model (3.7), the conditions of the minimax theorem (see e.g., [18] Chapter 6, Proposition 2.4) are all satisfied. That is, the constraints of flows are convex, and the energy function is linear in both the primal and dual functions $p_s(x)$, $p_t(x)$, $p(x)$ and $\lambda(x)$, hence convex l.s.c. for fixed λ and concave u.s.c. for fixed p_s, p_t and p. This also implies the existence of at least one saddle point, see [18]. It also follows that the min and max operators in the above primal-dual model (3.7) can be interchanged, i.e.

$$\sup_{p_s,p_t,p} \inf_{\lambda} E(p_s,p_t,p;\lambda) \,=\, \inf_{\lambda} \sup_{p_s,p_t,p} E(p_s,p_t,p;\lambda)\,. \tag{3.8}$$

Clearly, optimizing the primal-dual problem over the dual variable $\lambda(x)$ leads back to the primal max-flow model (3.5), i.e.

$$P(p_s,p_t,p) \,=\, \inf_{\lambda} E(p_s,p_t,p;\lambda)\,.$$

3.3. Dual Model: Continuous Min-Cut. We show in this section that optimizing the primal-dual model (3.6) or (3.7) over the flow variables p_s, p_t and p leads to its equivalent dual model:

$$\min_{\lambda(x)\in[0,1]} \Big\{ D(\lambda) \,=\, \int_\Omega \big\{ \big(1-\lambda(x)\big)C_s(x) + \lambda(x)C_t(x)\,dx + C(x)\,|\nabla\lambda(x)|\,\big\}\,dx \Big\}\,. \tag{3.9}$$

3.3.1. Optimization of Flow Variables. In order to optimize the flow variables of (3.7), let us first consider the following maximization problem

$$f(q) \;=\; \sup_{p \le C} \; p \cdot q \,. \tag{3.10}$$

When $q < 0$, p can be chosen to be negative infinity in order to maximize the value $p \cdot q$, which results in $f(q) = +\infty$. We further observe that

$$\begin{cases} \text{if } q = 0\,, & \text{then } p \le C \text{ and } f(q) \text{ reaches maximum } 0 \\ \text{if } q > 0\,, & \text{then } p = C \text{ and } f(q) \text{ reaches maximum } q \cdot C \end{cases} \quad . \tag{3.11}$$

Therefore, we can equally express $f(q)$ as

$$f(q) = \begin{cases} q \cdot C & \text{if } q \ge 0 \\ \infty & \text{if } q < 0 \end{cases} \tag{3.12}$$

Obviously, the function $f(q)$ given by (3.10) provides a prototype to maximize *primal-dual model* (3.7) over the source flow $p_s(x)$ and sink flow $p_t(x)$. Define

$$f_s(x) \;=\; \sup_{p_s(x) \le C_s(x)} \big(1 - \lambda(x)\big) \cdot p_s(x), \tag{3.13}$$

and

$$f_t(x) = \sup_{p_t(x) \le C_t(x)} \lambda(x) \cdot p_t(x)$$

$$. \tag{3.14}$$

Then, by the discussion above, for each position $x \in \Omega$:

$$f_s(x) = \begin{cases} \big(1 - \lambda(x)\big) \cdot C_s(x) & \text{if } \big(1 - \lambda(x)\big) \ge 0 \\ \infty & \text{if } \big(1 - \lambda(x)\big) < 0 \end{cases} \tag{3.15}$$

and

$$f_t(x) = \begin{cases} \lambda(x) \cdot C_t(x) & \text{if } \lambda(x) \ge 0 \\ \infty & \text{if } \lambda(x) < 0 \end{cases} \tag{3.16}$$

For the maximization of (3.7) over the spatial flow $p(x)$, it is well known that [20]

$$\sup_{|p(x)| \le C(x)} \int_\Omega \lambda \,\mathrm{div}\, p \, dx \;=\; \int_\Omega C \,|\nabla \lambda| \; dx \,. \tag{3.17}$$

By (3.15), (3.16) and (3.17), maximization of the primal-dual model (3.7) over flows p_s, p_t and p leads to its equivalent dual model (3.9). Observe that optimal λ must be contained in $[0, 1]$, otherwise the primal-dual energy would be infinite, contradicting the existence of at least one saddle point.

We summarize the above discussions by the following proposition:

PROPOSITION 3.1. *The continuous max-flow model* (3.5)*, the primal-dual model* (3.6) *or* (3.7) *and the dual model* (3.9) *are equivalent to each other.*

3.3.2. 'Saturated'/'Unsaturated' Flows and Cuts. In fact, the above discussions on (3.10) gives rise to a variational perspective of the connections of flows and cuts and also recovers related conceptions and terminologies used in graph-cut based approaches.

Let p^* be an optimum of (3.10). By means of variations, if $p^* < C$ strictly, its variation δp can be both positive and negative. Observe that if $p^* + \delta p$ doesn't increase the value $f(q)$ for any δp, it directly follows that $q = 0$. On the other hand, for $p^* = C$, variations δp under the constraint must satisfy $\delta p < 0$. Again, any $p^* + \delta p$ doesn't increase the value $f(q)$, hence it follows that $q \geq 0$. In other words, if the flow $p^* < C$ does not reach its maximum capacity, then $q = 0$ and $f(q) = 0$ and hence there is no contribution to the total energy. We say the corresponding edge is 'unsaturated' and is therefore not part of the 'minimal cut'.

We can explain the relationships between flows and cuts in the spatially continuous setting in the same manner. Let p_s^*, p_t^*, p^* and $\lambda^*(x)$ be an optimal primal-dual pair of (3.6).

Source Flows, Sink Flows and Cuts: Observe from (3.2) that if the source flow $p_s^*(x) < C_s(x)$ at $x \in \Omega$ is 'unsaturated', we must have $1 - \lambda^*(x) = 0$, i.e.

$$p_s^*(x) < C_s(x) \implies \lambda^*(x) = 1 \,.$$

At the position x, it is definitely labeled as 1. In addition, $f_s(x) = (1 - \lambda^*(x))p_s^*(x) = 0$, which means that at the position x, the source flow $p_s^*(x)$ has no contribution to the cut energy. It follows that $p_t^*(x) = C_t(x)$ is saturated and the minimal cut passes through the edge from x to the sink t.

Likewise, if the sink flow $p_t^*(x) < C_t(x)$ is 'unsaturated', we must have $\lambda^*(x) = 0$, i.e.

$$p_t^*(x) < C_t(x) \implies \lambda^*(x) = 0 \,.$$

At the position x, it is labeled as 0. In addition, $f_t(x) = \lambda^*(x)p_s^*(x) = 0$, which means that at the position x, the sink flow $p_t^*(x)$ has no contribution to the cut energy. Hence, $p_s^*(x) = C_s(x)$ is saturated and the minimal cut passes through the edge from the source s to x.

As we see, only 'saturated' source and sink flows have contributions to the total energy.

Spatial Flows and Cuts: for the spatial flows $p^*(x)$, let

$$C_{\mathrm{TV}}^{\alpha} := \{p \,|\, \|p\|_{\infty} \leq \alpha \,,\, p_n|_{\partial\Omega} = 0\} \,.$$

Observe that

$$\sup_{p \in C_{\mathrm{TV}}^{\alpha}} \langle \operatorname{div} p, \lambda \rangle = \sup_{p \in C_{\mathrm{TV}}^{\alpha}} \langle p, \nabla\lambda \rangle \,, \tag{3.18}$$

where the inner product $\langle a, b \rangle$ is $\int_{\Omega} a(x)b(x)\,dx$. The extremum of the inner product $\langle p^*, \nabla\lambda^* \rangle$ in (3.18) just indicates the normal cone-based condition [24] of $\nabla\lambda^*$, i.e.

$$\nabla\lambda^* \;\in\; N_{C_{\mathrm{TV}}^{\alpha}}(p^*) \,. \tag{3.19}$$

Then we simply have:

$$\text{if} \quad \nabla\lambda^*(x) \neq 0 \,, \qquad \text{then} \quad |p^*(x)| = \alpha \,, \tag{3.20a}$$

$$\text{if} \quad |p^*(x)| < \alpha \,, \qquad \text{then} \quad \nabla\lambda^*(x) = 0 \,. \tag{3.20b}$$

In other words, at potential cut locations $x \in \Omega$ where $\nabla\lambda^*(x) \neq 0$ the spatial flow $p^*(x)$ is 'saturated'. At locations $x \in \Omega$ where $|p(x)| < \alpha$ is not saturated we must have $\nabla\lambda^*(x) = 0$ and therefore the cut does not sever the spatial domain at x.

3.4. Global Binary Optimums of the Continuous Min-Cut. When $C(x)$ is constant over the whole image domain Ω, e.g. $C(x) = \alpha$, the dual model (3.9) is reduced to

$$\min_{\lambda(x)\in[0,1]} \Big\{ D(\lambda) \,=\, \int_\Omega \big\{ \big(1-\lambda(x)\big) C_s(x) + \lambda(x) C_t(x) + \alpha\,|\nabla\lambda(x)|\,\big\}\,dx \Big\} \tag{3.21}$$

which just coincides with the continuous min-cut model investigated by Chan et al [15]. When $C(x) \geq 0$ is some general function, e.g. the so-called edge detector, (3.9) amounts to the geodesic model studied by Bresson et al [11].

In this paper, we focus on the case that $C(x) = \alpha$ is constant for simplicity, and prove that there exists a series of binary optimums of (3.21) which are also globally optimal to the nonconvex min-cut problem (1.1) and can be obtained by thresholding. This is the same result as was shown by Chan et al [15]. We demonstrate it in another way by duality through the continuous max-flow model (3.5). We show that every such minimal cut of (1.1) has the same energy as the maximum flow energy of (3.5). The results can be easily extended to a more general version of (3.9) with non-constant $C(x)$.

PROPOSITION 3.2. *Let p_s^*, p_t^*, p^* and $\lambda^*(x)$ be a global optimum of the primal-dual model* (3.6) *when $C(x) = \alpha$. Then each $\ell-$upper level set $S^\ell := \{x \,|\, \lambda^*(x) \geq \ell,\ \ell \in (0,1]\}$, $\ell \in (0,1]$, of $\lambda^*(x)$ and the indicator function u^ℓ*

$$u^\ell(x) := \begin{cases} 1\,, & \lambda^*(x) \geq \ell \\ 0\,, & \lambda^*(x) < \ell \end{cases},$$

is a global binary solution of the nonconvex min-cut problem (1.1)*.*

Moreover, each cut energy given by S^ℓ has the same energy as its optimal max-flow energy, i.e.

$$P(p_s^*, p_t^*, p^*) \,=\, \int_\Omega p_s^*(x)\,dx\,.$$

Proof. Let p_s^*, p_t^*, p^* and $\lambda^*(x)$ be the optimal primal-dual pair of (3.6), then p_s^*, p_t^*, p^* optimize the max-flow problem (3.5) and $\lambda^*(x)$ optimizes the dual problem (3.21). Clearly, the maximal flow energy of (3.5) is

$$P(p_s^*, p_t^*, p^*) \,=\, \int_\Omega p_s^*(x)\,dx \tag{3.22}$$

and satisfies

$$P(p_s^*, p_t^*, p^*) \,=\, E(p_s^*, p_t^*, p^*; \lambda^*) \,=\, D(\lambda^*)\,.$$

For the max-flow problem (3.5), the flow conservation condition (3.4) is satisfied, i.e.

$$\operatorname{div} p^*(x) - p_s^*(x) + p_t^*(x) \,=\, 0\,, \quad \text{a.e. } x \in \Omega \tag{3.23}$$

Let S^ℓ be any level set of λ^* and $\ell \in (0,1]$ and u^ℓ be its indicator function. In view of (3.11), for any point $x \in \Omega\backslash S^\ell$, i.e. where $\lambda(x) < \ell \leq 1$, it is easy to see that

$$p_s^*(x) \,=\, C_s(x)\,, \quad \forall x \in \Omega. \tag{3.24}$$

Likewise, for any point $x \in S^\ell$, i.e. $\lambda(x) \geq \ell > 0$, we have

$$p_t^*(x) \,=\, C_t(x), \quad \forall x \in \Omega.$$

Then by (3.23), we have

$$p_s^*(x) \;=\; C_t(x) + \operatorname{div} p^*(x)\,, \quad x \in S^\ell, \quad \text{a.e. } x \in \Omega \tag{3.25}$$

Therefore, by (3.24) and (3.25), the total energy defined in (3.22), for each level set S^ℓ, is

$$\begin{aligned} P(p_s^*, p_t^*, p^*) \;&= \int_{\Omega\setminus S^\ell} C_s(x)\,dx + \int_{S^\ell} \big(C_t(x) + \operatorname{div} p^*(x)\big)\,dx \\ &= \int_{\Omega\setminus S^\ell} C_s(x)\,dx + \int_{S^\ell} C_t(x)\,dx + \int_{S^\ell} \operatorname{div} p^*(x)\,dx \\ &= \int_{\Omega\setminus S^\ell} C_s(x)\,dx + \int_{S^\ell} C_t(x)\,dx + \alpha\left|\partial S^\ell\right|\,. \end{aligned}$$

The last term follows from the fact that $p_n^*(x) = \alpha$ at $\forall x \in \partial S^\ell$ and the Gaussian theorem

$$\int_{S^\ell} \operatorname{div} p^*(x)\,dx \;=\; \int_{\partial S^\ell} p_n^*(x)\,dl \;=\; \alpha\left|\partial S^\ell\right|\,. \tag{3.26}$$

Therefore, the binary function u^ℓ, which is the indicator function of S^ℓ, solves the nonconvex min-cut problem (1.1) globally. This can be seen by the facts: u^ℓ is obviously obtained in the relaxed convex set $\lambda(x) \in [0,1]$ and its energy $P(p_s^*, p_t^*, p^*)$ is globally optimal to both convex relaxed models (3.5) and (3.21). □

In other words, the continuous max-flow formulation (3.5) implicitly leads to a segmentation of Ω with minimal length, i.e. the continuous min-cut given by the optimal multiplier function $\lambda^*(x)$. In this respect, the continuous max-flow model (3.5) solves the nonconvex segmentation model (1.1) globally and exactly, which provides a clue to build up the novel max-flow based algorithm in Sec. 5.1.

4. Supervised Continuous Max-Flow and Min-Cut. In this section, we study continuous max-flow and min-cut models with priori given supervision constraints.

In contrast to the continuous max-flow and min-cut introduced above, the supervised max-flow/min-cut computes the optimal partition subject to given constraints on region configurations, e.g. some image pixels are labeled in advance as foreground or background. This gives a supervised image partitioning problem which can be modeled as the following *supervised continuous min-cut problem*

$$\begin{aligned} &\min_{S} \;\int_{S\setminus\Omega_f} C_s(x)\,dx + \int_{(\Omega\setminus\Omega_b)\setminus S} C_t(x)\,dx + \alpha\,|\partial S| \\ &\text{s.t. } \; \Omega_f \subset S \subset \Omega\setminus\Omega_b \end{aligned} \tag{4.1}$$

where $\Omega_f, \Omega_b \subset \Omega$ are the two disjoint areas marked a priori by the user: Ω_f belongs to the foreground or objects and Ω_b belongs to the background.

The supervised continuous min-cut formulation can be equivalently be written in terms of the binary characteristic function $\lambda(x) \in \{0,1\}$:

$$\min_{\lambda(x)\in\{0,1\}} \int_\Omega (1-\lambda(x))C_s(x)\,dx \;+\; \int_\Omega \lambda(x)C_t(x)\,dx \;+\; \alpha\int_\Omega |\nabla\lambda(x)|\;dx\,. \tag{4.2}$$

subject to the labeling constraints

$$\lambda(\Omega_f) \;=\; 1\,, \quad \lambda(\Omega_b) \;=\; 0\,. \tag{4.3}$$

Consider the above discussions in Sec. 3, we may simply set

$$C_s(\Omega_f) \,=\, +\infty\,, \quad C_t(\Omega_b) \,=\, +\infty\,. \tag{4.4}$$

This says that the source flow $p_s(x)$ is not constrained at $x \in \Omega_f$ and the sink flow $p_t(x)$ is not constrained at $x \in \Omega_b$. In view of discussions of Sec. 3.3.1, the labeling constraints (4.3) would then follow. As in [8], this provides a direct way to couple the max-flow approach to the min-cut problem with supervised constraints (4.3).

In this work, we also propose new supervised max-flow and min-cut models without the artificial flow constraints (4.4), which implicitly encode the supervised information (4.3) and share the same complexities as the unsupervised formulations: (3.5) and (3.9). It is also flexible in case the supervised information is not given in a determinant way as (4.3): for example the marked areas Ω_f and Ω_b may be provided in a 'soft' manner by probabilities:

$$\lambda(\Omega_f) \,=\, t_f \,\in\, (0,1)\,, \quad \lambda(\Omega_b) \,=\, t_b \,\in\, (0,1) \tag{4.5}$$

where t_f and t_b are positive constants but less than 1. It is easy to see that modifying the flows manually by (4.4) does not work in this case.

To motivate the following approach, we first define two characteristic functions concerning the label constraints (4.3):

$$u_f(x) = \left\{ \begin{array}{ll} 1, & x \in \Omega_f \\ 0, & x \notin \Omega_f \end{array} \right. , \quad u_b(x) = \left\{ \begin{array}{ll} 0, & x \in \Omega_b \\ 1, & x \notin \Omega_b \end{array} \right. . \tag{4.6}$$

Observe that Ω_f and Ω_b are disjoint, it follows that

$$u_f(\Omega_b) \,=\, 0\,, \quad u_b(\Omega_f) \,=\, 1\,. \tag{4.7}$$

For the 'soft' version of the constraints (4.5), we define

$$u_f(x) = \left\{ \begin{array}{ll} t_f, & x \in \Omega_f \\ 0, & x \notin \Omega_f \end{array} \right. , \quad u_b(x) = \left\{ \begin{array}{ll} 1-t_b, & x \in \Omega_b \\ 1, & x \notin \Omega_b \end{array} \right. . \tag{4.8}$$

It is easy to see that the functions $u_f(x)$ and $u_b(x)$ describe the lower and upper bounds of the probability of labeling the image pixel $x \in \Omega$ as foreground objective. This is further shown in Sec. 4.3.

In the following discussions, we still focus on the case when (4.3) to ease the derivions. The results can be simply extended to the case of (4.5).

4.1. Primal Model: Supervised Max-Flow. We propose the new supervised max-flow model as follows:

Consider the source flow $p_s(x)$, which flows from the source s to each pixel $x \in \Omega$; when $x \in \Omega_b$, the flow should have no contribution to the energy as it passes through the known background pixel; otherwise, it is valued as the full flow $p_s(x)$. Therefore, in view of (4.6) which implies $u_b(\Omega_b) \,=\, 0$ and $u_b(\Omega \backslash \Omega_b) \,=\, 1$, the total source flow p_s in Ω is given by $\int_\Omega \, u_b(x) p_s(x)\, dx$. Concerning the total cost of the sink flow $p_t(x)$: it flows from each spatial pixel x to the sink t; when $x \in \Omega_f$, the sink flow costs $-p_t(x)$ where its negative sign means it reduces the cost; otherwise, sink flow costs nothing, likewise, in view of (4.6) where $u_f(\Omega_f) \,=\, 1$ and $u_f(\Omega \backslash \Omega_f) \,=\, 0$, we can value the total cost of p_t in Ω by $-\int_\Omega \, u_f(x) p_t(x)\, dx$.

In contrast to the *continuous max-flow* problem (3.5), we formulate the related *supervised max-flow model* as

$$\sup_{p_s, p_t, p} \; P_S(p_s, p_t, p) \,=\, \int_\Omega \, u_b(x) p_s(x)\, dx - \int_\Omega \, u_f(x) p_t(x)\, dx \tag{4.9}$$

subject to the same flow constraints (3.1), (3.2), (3.3) and (3.4) on p_s, p_t and p. Likewise, (4.9) is also called the primal model of the supervised max-flow / min-cut problem.

As the special case when no priori information about foreground and background is given, then we have the two characteristic functions $u_f(x) = 0$ and $u_b(x) = 1$ for $\forall x \in \Omega$. It is easy to check that the supervised max-flow problem (4.9) coincides with the max-flow problem (3.5) in this case.

4.2. Supervised Primal-Dual Model. In analogue with (3.6), we can construct the equivalent primal-dual formulation of (4.9) by introducing the multiplier function λ

$$\begin{aligned} \sup_{p_s,p_t,p} \inf_{\lambda} E_S(p_s,p_t,p;\lambda) \;=\; & \int_\Omega u_b(x)p_s(x)\,dx - \int_\Omega u_f(x)p_t(x)\,dx + \\ & \int_\Omega \lambda(x)\big(\operatorname{div} p(x) - p_s(x) + p_t(x)\big)\,dx \\ \text{s.t.}\quad & p_s(x) \le C_s(x)\,,\; p_t(x) \le C_t(x)\,,\; |p(x)| \;\le\; C(x)\,, \end{aligned} \tag{4.10}$$

which can be equivalently be formulated by

$$\begin{aligned} \sup_{p_s,p_t,p} \inf_{\lambda} E_S(p_s,p_t,p;\lambda) \;=\; & \int_\Omega (u_b-\lambda)p_s\,dx + \int_\Omega (\lambda-u_f)p_t\,dx + \\ & \int_\Omega \lambda(x)\operatorname{div} p(x)\,dx \\ \text{s.t.}\quad & p_s(x) \le C_s(x)\,,\; p_t(x) \le C_t(x)\,,\; |p(x)| \;\le\; C(x)\,. \end{aligned} \tag{4.11}$$

As discussed in section 3.2, we have the same minimax relationship as (3.8), i.e.

$$\sup_{p_s,p_t,p} \inf_{\lambda} E_S(p_s,p_t,p;\lambda) \;=\; \inf_{\lambda} \sup_{p_s,p_t,p} E_S(p_s,p_t,p;\lambda)\,,$$

and at least one optimal primal-dual saddle point exist.

4.3. Dual Model: Supervised Min-Cut. Maximizing all the flow functions p_s, p_t and p in $E_S(p_s,p_t,p;\lambda)$ of (4.11), in the same manner as (3.15), (3.16) and (3.17), leads to the equivalent dual model to (4.9), also called the *supervised min-cut model* in this paper:

$$\begin{aligned} \min_{\lambda} D_S(\lambda) \;=\; & \int_\Omega \big(u_b-\lambda\big)C_s\,dx + \int_\Omega \big(\lambda-u_f\big)C_t\,dx \;+ \int_\Omega C(x)\,|\nabla\lambda(x)|\;dx \\ \text{s.t.}\quad & u_f(x) \;\le\; \lambda(x) \;\le\; u_b(x)\,. \end{aligned} \tag{4.12}$$

In this paper, we focus on the case that $C(x) = \alpha$, $\forall x \in \Omega$, then (4.12) can be equally written as

$$\begin{aligned} \min_{\lambda} D_S(\lambda) \;=\; & \int_\Omega \big(u_b-\lambda\big)C_s\,dx + \int_\Omega \big(\lambda-u_f\big)C_t\,dx + \alpha\int_\Omega |\nabla\lambda(x)|\;dx \\ \text{s.t.}\quad & u_f(x) \;\le\; \lambda(x) \;\le\; u_b(x)\,; \end{aligned} \tag{4.13}$$

or, observe u_b and u_f are given in advance, be shortened as

$$\begin{aligned} \min_{\lambda} D_S(\lambda) \;=\; & \int_\Omega \lambda\big(C_t-C_s\big)\,dx + \alpha\int_\Omega |\nabla\lambda(x)|\;dx \\ \text{s.t.}\quad & u_f(x) \;\le\; \lambda(x) \;\le\; u_b(x)\,. \end{aligned} \tag{4.14}$$

We see that (4.14) is just the convex relaxed model of the nonconvex supervised min-cut problem (4.2), where the subset ordering

$$\Omega_f \subset S \subset \Omega \backslash \Omega_b$$

in (4.1) is expressed by the inequality ordering

$$u_f(x) \leq \lambda(x) \leq u_b(x)\,, \quad x \in \Omega$$

in (4.14).

Moreover, the applied inequality constraint of λ in (4.14), in view of (4.6) and (4.7), just gives

$$\lambda(\Omega_f) = 1\,, \quad \lambda(\Omega_b) = 0\,. \tag{4.15}$$

This coincides with the priori information that Ω_f is already labeled as foreground objects and Ω_b is labeled as the background. It follows that the inequality constraint of $\lambda(x)$ implicitly encodes the priori supervision information.

In the special case when no priori information about foreground and background is given, i.e. $u_f(x) = 0$ and $u_b(x) = 1\ \forall x \in \Omega$, it is easy to see that the supervised min-cut problem (4.13) is equivalent to the continuous min-cut problem (1.2).

4.4. Global Binary Supervised Min-Cuts. Now we prove that global optimums of the nonconvex supervised min-cut model (4.1) can also be obtained by taking each upper level set of the global optimum λ^* to its convex relaxed version (4.13) or (4.14), in a similar manner as Prop. 3.2.

PROPOSITION 4.1. *Let p_s^*, p_t^*, p^* and $\lambda^*(x)$ be a global optimum of the primal-dual problem* (4.10) *with $C(x) = \alpha$. Then each $\ell-$upper level set $S^\ell := \{x \,|\, \lambda(x) \geq \ell\}$ of $\lambda^*(x)$ where $\ell \in (0, 1]$, and its indicator function u^ℓ:*

$$u^\ell(x) := \begin{cases} 1\,, & \lambda^*(x) \geq \ell \\ 0\,, & \lambda^*(x) < \ell \end{cases},$$

is a global solution of the nonconvex supervised min-cut problem (4.1)*.*

Moreover, each supervised cut given by S^ℓ has the same energy as the optimal supervised max-flow energy, i.e.

$$P_S(p_s^*, p_t^*, p^*) = \int_\Omega u_b(x) p_s^*(x)\, dx - \int_\Omega u_f(x) p_t^*(x)\, dx\,.$$

Proof. Let p_s^*, p_t^*, p^* and $\lambda^*(x)$ be a global optimum of (4.10). Then p_s^*, p_t^*, p^* optimize the primal problem (4.9) and $\lambda^*(x)$ optimizes (4.13) or (4.14) at the same time. Meanwhile, the two energies are equal, i.e.

$$P_S(p_s^*, p_t^*, p^*) = E_S(p_s^*, p_t^*, p^*, \lambda^*) = D_S(\lambda^*)\,.$$

By the definition of u_b and u_f in (4.6), the optimal energy of (4.9) is

$$\begin{aligned} P_S(p_s^*, p_t^*, p^*) &= \int_\Omega u_b(x) p_s^*(x)\, dx - \int_\Omega u_f(x) p_t^*(x)\, dx \\ &= \int_{\Omega \backslash \Omega_b} p_s^*(x)\, dx - \int_{\Omega_f} p_t^*(x)\, .dx \end{aligned} \tag{4.16}$$

Concerning the supervised min-cut problem, (4.15) indicates that

$$\lambda^*(\Omega_f) \,=\, 1\,, \quad \lambda^*(\Omega_b) \,=\, 0\,. \tag{4.17}$$

Then each level set S^ℓ $\ell \in (0,1]$,

$$S^\ell \,:=\, \{x \,|\, \lambda^*(x) \,\geq\, \ell\,\}\,,$$

of λ^* contains Ω_f and excludes Ω_b, i.e. we have

$$\Omega_f \,\subset\, S^\ell \,\subset\, \Omega\backslash\Omega_b\,. \tag{4.18}$$

As $\lambda^*(x)$ is the optimal multiplier, we must have the flow conservation condition (3.4), i.e.

$$\operatorname{div} p^*(x) - p_s^*(x) + p_t^*(x) \,=\, 0, \quad \text{a.e. } x \in \Omega. \tag{4.19}$$

For any point $x \in S^\ell$, i.e. where $\lambda^*(x) \geq \ell$, we have by (4.17) that $\lambda^*(x) \geq u_f(x)$, and therefore

$$p_t^*(x) \,=\, C_t(x)\,.$$

Then by (4.19), we have

$$p_s^*(x) \,=\, C_t(x) + \operatorname{div} p^*(x)\,, \quad \text{a.e. } x \in S^\ell\backslash\Omega_f\,. \tag{4.20}$$

And for any point $x \in (\Omega\backslash\Omega_b)\backslash S^\ell$, i.e. $\lambda^*(x) < \ell$, hence $\lambda^*(x) < u_b(x)$ and it is easy to see that

$$p_s^*(x) \,=\, C_s(x)\,. \tag{4.21}$$

Therefore, in view of (4.21) and (4.20), the total optimal energy (4.16) is

$$\begin{aligned} P_S(p_s^*, p_t^*, p^*) \,&=\, \int_{(\Omega\backslash\Omega_b)\backslash S^\ell} C_s(x)\,dx + \int_{S^\ell} \big(C_t(x) + \operatorname{div} p^*(x)\big)\,dx - \int_{\Omega_f} p^*(x)dx \\ &= \int_{(\Omega\backslash\Omega_b)\backslash S^\ell} C_s(x)\,dx + \int_{S^\ell\backslash\Omega_f} C_t(x)\,dx + \int_{S^\ell} \operatorname{div} p^*(x)\,dx \\ &= \int_{(\Omega\backslash\Omega_b)\backslash S^\ell} C_s(x)\,dx + \int_{S^\ell\backslash\Omega_f} C_t(x)\,dx + \alpha\left|\partial S^\ell\right|\,, \end{aligned}$$

which obviously gives a solution u^ℓ of the nonconvex supervised min-cut problem (4.1). The last term follows from the observation of (3.26).

The above binary solution u^ℓ is contained in the relaxed convex set $\lambda(x) \,\in\, [0,1]$ and reaches the globally optimal energy E^*. It follows that such binary solver is globally optimal. □

5. Algorithms. In this section, we propose the new algorithms for the continuous min-cuts (1.2) and (4.14) based their respective max-flow formulations (3.5) and (4.9).

5.1. Continuous Max-Flow Based Algorithm. We motivate the algorithm upon the proposed continuous max-flow model (3.5). The energy function of its equivalent primal-dual model (3.6) is just the lagrangian function of (3.5). For such a linear equality constrained optimization problem, we derive our fast max-flow based algorithm by means of the augmented lagrangian method [6], which introduces an approach to compute both the flows and labeling function simultaneously. To this end, in view of the lagrangian function (3.6), we define the respective augmented lagrangian function as

$$L_c(p_s, p_t, p, \lambda) := \int_\Omega p_s \, dx + \int_\Omega \lambda\big(\operatorname{div} p - p_s + p_t\big)\, dx - \frac{c}{2} \|\operatorname{div} p - p_s + p_t\|^2 , \quad (5.1)$$

where $c > 0$. Alg. 5.1 shows the details of the proposed continuous max-flow based algorithm, where $\lambda(x)$ is updated as the multiplier at each iteration. Alg. 5.1 is an example of the alternating direction method of multipliers. Convergence can be validated by optimization theories.

The sub-minimization problem (5.2) can also be solved by one step of the following iterative procedure:

$$p^{k+1} = \Pi_\alpha\Big(p^k + c\nabla(\operatorname{div} p^k - F^k).\Big) \quad (5.3)$$

where Π_α is the convex projection onto the convex set $C_\alpha = \{q \,|\|q\|_\infty \le \alpha\}$. This requires much less computational efforts.

5.2. Supervised Continuous Max-Flow Based Algorithm. Now we propose the algorithm for the supervision-constrained min-cut problem (4.14) based upon its equivalent continuous max-flow formulation (4.9). Likewise, its equivalent primal-dual formulation of (4.10) is obviously just the lagrangian function of (4.9). We define its respective augmented lagrangian function as

$$\begin{aligned} L_c(p_s, p_t, p, \lambda) \;=\; & \int_\Omega u_b p_s \, dx - \int_\Omega u_f p_t \, dx + \int_\Omega \lambda\big(\operatorname{div} p - p_s + p_t\big)\, dx \\ & - \frac{c}{2} \|\operatorname{div} p - p_s + p_t\|^2 . \end{aligned}$$

where $c > 0$.

The supervised continuous max-flow based algorithm is stated in Alg. 5.2.

6. Experiments. We show two types of experiments for the proposed continuous max-flow / min-cut models: unsupervised image segmentation and supervised image segmentation.

6.1. Unsupervised Image Segmentation. For image segmentation without user inputs, we adopt piecewise constant functions as the image model: i.e. two grayvalues f_1 and f_2 are chosen priori for clues to build data terms:

$$C_s(x) \;=\; D(f(x) - f_1(x))\,, \quad C_t(x) \;=\; D(f(x) - f_2(x))\,,$$

where $D(\cdot)$ is some penalty function.

Fig. 6.1 and Fig. 6.2 show two experiments. Each is computed by the proposed continuous max-flow based method Alg. 5.1 and Bresson et al [11] for comparisons. For the experiment shown in Fig. 6.1, we chose $\alpha = 0.4$ and threshhold value $\ell = 0.5$. Our method converges to a result (see graphs at the second row of Fig. 6.1), which takes the value 0 or

Algorithm 1 Multiplier-Based Maximal-Flow Algorithm

Set the starting values p_s^1, p_t^1, p^1 and λ^1, let $k = 1$ and start $k-$th iteration, which includes the following steps, until convergence:

- Optimizing p by fixing other variables

$$\begin{aligned} p^{k+1} &:= \arg \max_{\|p\|_\infty \leq \alpha} L_c(p_s^k, p_t^k, p, \lambda^k)\,. \\ &= \arg \max_{\|p\|_\infty \leq \alpha} -\frac{c}{2} \left\|\operatorname{div} p(x) - F^k\right\|^2 , \end{aligned} \tag{5.2}$$

  where F^k is a fixed variable. This problem can either be solved iteratively by Chambolle's projection algorithm [13], or approximately by one step of (5.3).

- Optimizing p_s by fixing other variables

$$\begin{aligned} p_s^{k+1} &:= \arg \max_{p_s(x) \leq C_s(x)} L_c(p_s, p_t^k, p^{k+1}, \lambda^k) \\ &:= \arg \max_{p_s(x) \leq C_s(x)} \int_\Omega p_s\, dx - \frac{c}{2} \left\|p_s - G^k\right\|^2 \end{aligned}$$

  where G^k is a fixed variable and optimizing p_s can be easily computed at each $x \in \Omega$ pointwise;

- Optimizing p_t by fixing other variables

$$\begin{aligned} p_t^{k+1} &:= \arg \max_{p_t(x) \leq C_t(x)} L_c(p_s^{k+1}, p_t, p^{k+1}, \lambda^k) \\ &:= \arg \max_{p_t(x) \in C_t(x)} -\frac{c}{2} \left\|p_t - H^k\right\|^2 , \end{aligned}$$

  where H^k is a fixed variable and optimizing p_t can be simply solved by

$$p_t(x) \;=\; \min(H^k(x), C_t(x))\,;$$

- Update λ by

$$\lambda^{k+1} \;=\; \lambda^k - c\,(\operatorname{div} p^{k+1} - p_s^{k+1} + p_t^{k+1})\,;$$

- Let $k = k + 1$ go to the $k + 1$ iteration until converge.

1 nearly everywhere. This is in contrast to the result of the method by Bresson et al (see graphs at the first row of Fig. 6.1). For the experiment shown in Fig. 6.2, we chose $\alpha = 0.4$ and threshhold value $\ell = 0.02$. Both results look quite the same, but our method converges significantly faster than the algorithm of Bresson et al [11].

In all experiments, at each iteration we evaluate the following convergence criterion:

$$\text{err}^k \;=\; \left\|\lambda^{k+1} - \lambda^k\right\| / \left\|\lambda^{k+1}\right\| .$$

In contrast to Bresson et al [11], the proposed algorithm converges within 100 iterations (the accuracy below 1×10^{-4}). It greatly outperforms [11] in terms of convergence rate, see Fig. 6.3: Bresson et al (blue line) and ours (red line). In addition, our algorithm is also reliable for a wide range of c.

Algorithm 2 Multiplier-Based Supervised Max-Flow

Set the starting values p_s^1, p_t^1, p^1 and λ^1, let $k = 1$ and start $k-$th iteration, which includes the following steps, until convergence:

- Optimizing p by fixing other variables

$$\begin{aligned} p^{k+1} &:= \arg \max_{\|p\|_\infty \leq \alpha} L_c(p_s^k, p_t^k, p, \lambda^k) \\ &:= \arg \max_{\|p\|_\infty \leq \alpha} -\frac{c}{2} \left\| \operatorname{div} p - F^k \right\|^2 ; \end{aligned}$$

  where F^k is some fixed variable and results in a projection algorithm [13] or the gradient decent project (5.3);
- Optimizing p_s by fixing other variables

$$\begin{aligned} p_s^{k+1} &:= \arg \max_{p_s(x) \leq C_s(x)} L_c(p_s, p_t^k, p^{k+1}, \lambda^k) \\ &:= \arg \max_{p_s(x) \leq C_s(x)} \int_\Omega u_b p_s \, dx - \frac{c}{2} \left\| p_s - G^k \right\|^2 , \end{aligned}$$

  where G^k is a fixed variable and optimizing p_s can be easily computed at each $x \in \Omega$ pointwise;
- Optimizing p_t by fixing other variables

$$\begin{aligned} p_t^{k+1} &:= \arg \max_{p_t(x) \leq C_t(x)} L_c(p_s^{k+1}, p_t, p^{k+1}, \lambda^k) \\ &:= \arg \max_{p_t(x) \in C_t(x)} -\int_\Omega u_f p_t \, dx - \frac{c}{2} \left\| p_t - H^k \right\|^2 , \end{aligned}$$

  where H^k is a fixed variable and optimizing p_t can be also simply solved pointwise;
- Update λ by

$$\lambda^{k+1} \, = \, \lambda^k - c \, (\operatorname{div} p^{k+1} - p_s^{k+1} + p_t^{k+1}) \, ;$$

- Let $k = k + 1$ go to the $k + 1$ iteration until converge.

6.2. Supervised Image Segmentation. For supervised image segmentation, we use the Middlebury data set [43] for experiments, see images in Fig. 6.4. The corresponding data term, i.e. $C_s(x)$ and $C_t(x)$, is based on Gaussian mixture color models of foreground and background and provided in advance. It is not required for us to put very large flow capacities artificially at the marked areas Ω_f and Ω_b as proposed in the supervised continuous max-flow method (4.9). This in contrast to graph-based supervised image segmentation [45, 29, 10].

Here the tree-reweighted message passing method [45, 29] and α expansion method [10, 8] are applied for comparisons. As we see, there are no visual artifacts, like metrication errors, in our results (see details of the results, e.g. the left-bottom pedal of the flower (middle column)).

7. Conclusions and Future Topics. We study continuous max-flow and min-cut models, with or without supervised constraints, in this work. Dualities between max-flow and min-cut in the spatially continuous setting are set up and investigated by variational techniques. In this regard, terminologies used by graph-cut based techniques are revisited and explained under a new variational perspective. New optimization results on the exactness of

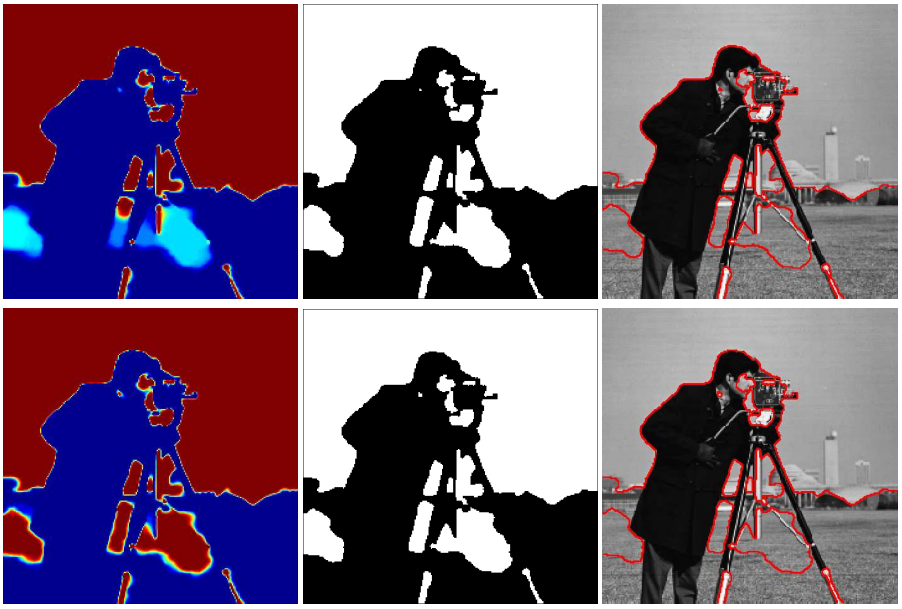

FIG. 6.1. *At this experiment, we chose* $\alpha = 0.4$ *and* $\ell = 0.5$. *Graphs of the first row show the results by Bresson et al: (left) computed* $\lambda^*(x)$, *(middle) threshholded* $u^\ell(x)$, *(right) segmented image. Graphs of the second row show the results by our method: (left) computed* $\lambda^*(x)$, *(middle) threshholded* $u^\ell(x)$, *(right) segmented image.*

the proposed convex models are derived and discussed with helps of the continuous max-flow formulations. The proposed continuous max-flow based algorithms are based upon classical convex optimization theories, which provide fast and reliable numerical schemes. In contrast to discrete graph-based methods, the algorithms can be easily speeded up by adopting a multigrid or parallel numerical scheme.

The max-flow methods can also be extended to other min-cut problems with multiple phases (see the companion of this work and [47]). It also paves the way to understand the classical graph based max-flow / min-cut algorithms in a completely variational manner. To this end, the proposed max-flow algorithmic scheme can also be generalized to solve min-cut problems over a regular weighted graph, where the cut information, i.e. labeling function, works as associated multipliers. This is one topic of our future studies.

Recently, the Split-Bregman method, a technique for solving unconstrained total variation problems has been applied to solve the convexified labeling problem (1.2), and was also shown to outperform the method of Bresson et al [11], see [22]. A detailed comparison with this method will be presented in another paper along with several fast implementations of our continuous max-flow algorithms.

REFERENCES

[1] Aseem Agarwala, Mira Dontcheva, Maneesh Agrawala, Steven Drucker, Alex Colburn, Brian Curless, David Salesin, and Michael Cohen. Interactive digital photomontage. *ACM Trans. Graph*, 23:294–302, 2004.

[2] Ben Appleton and Hugues Talbot. Globally optimal surfaces by continuous maximal flows. In *DICTA*, pages 987–996, 2003.

[3] Ben Appleton and Hugues Talbot. Globally minimal surfaces by continuous maximal flows. *IEEE Trans. Pattern Anal. Mach. Intell.*, 28(1):106–118, 2006.

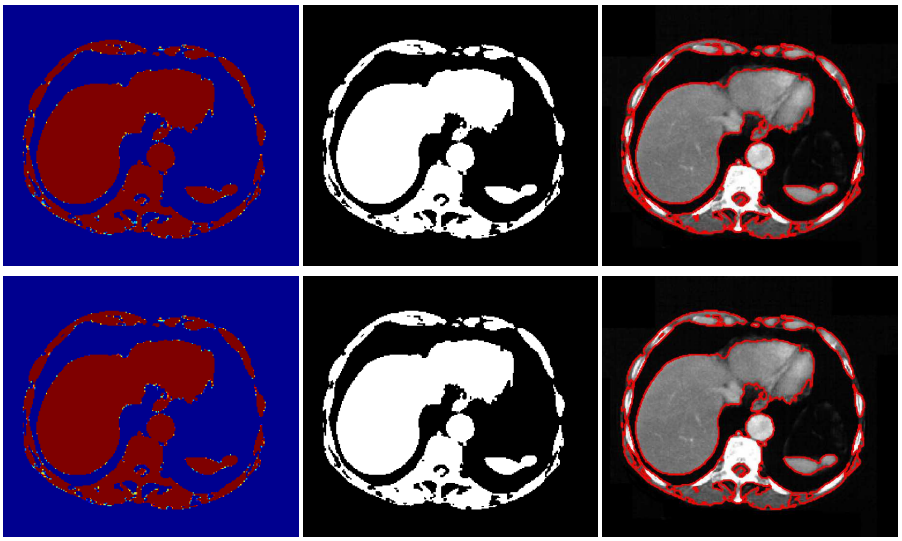

FIG. 6.2. *At this experiment, we chose* $\alpha = 0.02$ *and* $\ell = 0.5$. *Graphs of the first row show the results by Bresson et al: (left) computed* $\lambda^*(x)$, *(middle) threshholded* $u^\ell(x)$, *(right) segmented image. Graphs of the second row show the results by our method: (left) computed* $\lambda^*(x)$, *(middle) threshholded* $u^\ell(x)$, *(right) segmented image.*

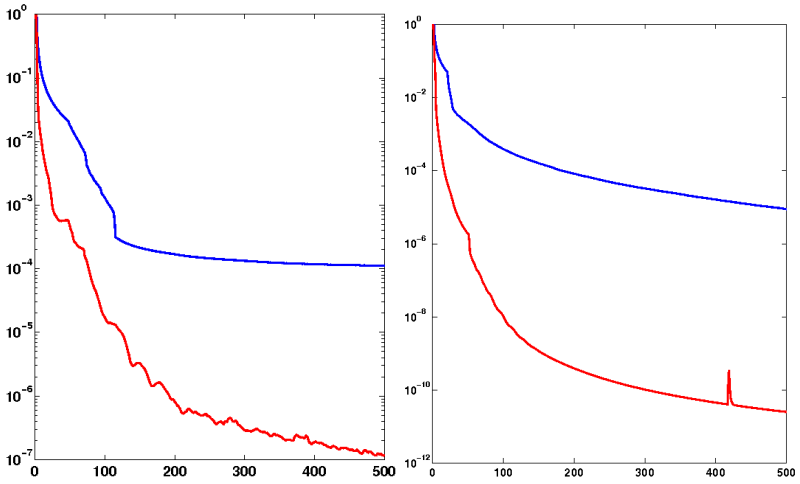

FIG. 6.3. *Comparisons of convergence: (***left***) for the experiment shown in Fig. 6.1, the method of Bresson et al (blue line) converges much slower than the proposed continuous max-flow method* (3.5)*(red line); (***right***) for the experiment shown in Fig. 6.2, the method of Bresson et al (blue line) also converges much slower than the proposed continuous max-flow method* (3.5)*(red line).*

[4] E. Bae, J. Yuan, and X.C. Tai. Global minimization for continuous multiphase partitioning problems using a dual approach. Technical report CAM09-75, UCLA, CAM, September 2009.

[5] Egil Bae and Xue-Cheng Tai. Efficient global minimization for the multiphase Chan-Vese model of image segmentation. In *Energy Minimization Methods in Computer Vision and Pattern Recognition (EMMCVPR)*, pages 28–41, 2009.

[6] Dimitri P. Bertsekas. *Nonlinear Programming*. Athena Scientific, September 1999.

[7] Endre Boros and Peter L. Hammer. Pseudo-boolean optimization. *Discrete Appl. Math.*, 123(1-3):155–225, 2002.

[8] Yuri Boykov and Vladimir Kolmogorov. An experimental comparison of min-cut/max-flow algorithms for

FIG. 6.4. **1st. row:** *The three given images, from the Middlebury data set, with pixels marked as foreground (white) and background (black).* **2nd row:** *computation result of λ^* to each image shown by color images,* 0*: blue and* 1*: red.* **3rd row:** *the black-white segmentation result by a threshhold of λ^*.* **4th and 5th rows:** *respective results computed from tree-reweighted message passing method [45, 29] and α expansion algorithm [10, 8].*

energy minimization in vision. *IEEE Transactions on Pattern Analysis and Machine Intelligence*, 26:359–374, 2001.

[9] Yuri Boykov and Vladimir Kolmogorov. Computing geodesics and minimal surfaces via graph cuts. In *ICCV*, pages 26–33, 2003.

[10] Yuri Boykov, Olga Veksler, and Ramin Zabih. Fast approximate energy minimization via graph cuts. *IEEE Transactions on Pattern Analysis and Machine Intelligence*, 23:1222 – 1239, 2001.

[11] Xavier Bresson, Selim Esedoglu, Pierre Vandergheynst, Jean-Philippe Thiran, and Stanley Osher. Fast global minimization of the active contour/snake model. *Journal of Mathematical Imaging and Vision*, 28(2):151–167, 2007.

[12] Vincent Caselles, Ron Kimmel, and Guillermo Sapiro. Geodesic active contours. In *ICCV*, pages 694–699, 1995.

[13] Antonin Chambolle. An algorithm for total variation minimization and applications. *Journal of Mathematical Imaging and Vision*, 20(1):89–97, January 2004.

[14] T. F. Chan and L. A. Vese. Active contours without edges. *Image Processing, IEEE Transactions on*, 10(2):266–277, 2001.

[15] Tony F. Chan, Selim Esedo ̄glu, and Mila Nikolova. Algorithms for finding global minimizers of image segmentation and denoising models. *SIAM J. Appl. Math.*, 66(5):1632–1648 (electronic), 2006.

[16] Thomas H Cormen, Charles E Leiserson, Ronald L Rivest, and Clifford Stein. *Introduction to Algorithms*. MIT Press, Cambridge, MA, second edition, 2001.

[17] Yefim Dinitz. Dinitz' algorithm: The original version and even's version. *Theoretical Computer Science*, pages 218–240, 2006.

[18] Ivar Ekeland and Roger Téman. *Convex analysis and variational problems*. Society for Industrial and Applied Mathematics, Philadelphia, PA, USA, 1999.

[19] L. R. Ford and D. R. Fulkerson. *Flows in Networks*. Princeton University Press, 1962.

[20] Enrico Giusti. *Minimal surfaces and functions of bounded variation*. Australian National University, Canberra, 1977.

[21] Andrew V. Goldberg and Robert E. Tarjan. A new approach to the maximum-flow problem. *J. ACM*, 35(4):921–940, October 1988.

[22] Tom Goldstein, Xavier Bresson, and Stanley Osher. Geometric applications of the split bregman method: Segmentation and surface reconstruction. Technical report CAM09-06, UCLA, CAM, 2009.

[23] D. M. Greig, B. T. Porteous, and A. H. Seheult. Exact maximum a posteriori estimation for binary images. *Journal of the Royal Statistical Society, Series B*, pages 271–279, 1989.

[24] Jean-Baptiste Hiriart-Urruty and Claude Lemaréchal. *Convex analysis and minimization algorithms. I*, volume 305 of *Grundlehren der Mathematischen Wissenschaften [Fundamental Principles of Mathematical Sciences]*. Springer-Verlag, Berlin, 1993. Fundamentals.

[25] Hiroshi Ishikawa. Higher-order clique reduction in binary graph cut. In *CVPR*, pages 2993–3000, 2009.

[26] Michael Kass, Andrew Witkin, and Demetri Terzopoulos. Snakes: Active contour models. *International Journal of Computer Vision*, 1(4):321–331, 1988.

[27] Pushmeet Kohli, M. Pawan Kumar, and Philip H.S. Torr. p^3 and beyond: Move making algorithms for solving higher order functions. *IEEE Transactions on Pattern Analysis and Machine Intelligence*, 31(9):1645–1656, 2009.

[28] Vladimir Kolmogorov. What metrics can be approximated by geo-cuts, or global optimization of length/area and flux. In *ICCV*, pages 564–571, 2005.

[29] Vladimir Kolmogorov. Convergent tree-reweighted message passing for energy minimization. *IEEE Trans. Pattern Anal. Mach. Intell.*, 28(10):1568–1583, 2006.

[30] Vladimir Kolmogorov and Carsten Rother. Minimizing nonsubmodular functions with graph cuts-a review. *IEEE Trans. Pattern Anal. Mach. Intell.*, 29(7):1274–1279, 2007.

[31] Vladimir Kolmogorov and Ramin Zabih. Multi-camera scene reconstruction via graph cuts. In *European Conference on Computer Vision*, pages 82–96, 2002.

[32] Vladimir Kolmogorov and Ramin Zabih. What energy functions can be minimized via graph cuts. *IEEE Transactions on Pattern Analysis and Machine Intelligence*, 26:65–81, 2004.

[33] Nikos Komodakis and Georgios Tziritas. Approximate labeling via graph-cuts based on linear programming. In *Pattern Analysis and Machine Intelligence*, pages 1436–1453, 2007.

[34] Vivek Kwatra, Arno Schoedl, Irfan Essa, Greg Turk, and Aaron Bobick. Graphcut textures: Image and video synthesis using graph cuts. *ACM Transactions on Graphics, SIGGRAPH 2003*, 22(3):277–286, July 2003.

[35] J. Lellmann, J. Kappes, J. Yuan, F. Becker, and C. Schnörr. Convex multi-class image labeling by simplex-constrained total variation. Technical report, HCI, IWR, Uni. Heidelberg, IWR, Uni. Heidelberg, November 2008.

[36] Victor Lempitsky and Yuri Boykov. Global optimization for shape fitting. In *CVPR, 2007. 6*, 2007.

[37] Victor S. Lempitsky, Yuri Boykov, and Denis V. Ivanov. Oriented visibility for multiview reconstruction. In *ECCV'06*, pages 226–238, 2006.

[38] Stan Z. Li. *Markov random field modeling in image analysis*. Springer-Verlag New York, Inc., Secaucus, NJ, USA, 2001.

[39] Nikos Paragios, Yunmei Chen, and Olivier Faugeras. *Handbook of Mathematical Models in Computer Vision*. Springer-Verlag New York, Inc., Secaucus, NJ, USA, 2005.

[40] T. Pock, A. Chambolle, H. Bischof, and D. Cremers. A convex relaxation approach for computing minimal partitions. In *IEEE Conference on Computer Vision and Pattern Recognition (CVPR)*, pages 810–817, Miami, Florida, 2009.

[41] Gil. Strang. Maximal flow through a domain. *Mathematical Programming*, 26:123–143, 1983.

[42] Gil. Strang. Maximum flows and minimum cuts in the plane. *Advances in Mechanics and Mathematics*, III:1–11, 2008.

[43] Richard Szeliski, Ramin Zabih, Daniel Scharstein, Olga Veksler, Aseem Agarwala, and Carsten Rother. A comparative study of energy minimization methods for markov random fields. In *ECCV*, pages 16–29, 2006.

[44] George Vogiatzis, Carlos H. Esteban, Philip H. Torr, and Roberto Cipolla. Multi-view stereo via volumetric graph-cuts and occlusion robust photo-consistency. *PAMI*, 29(12):2241–2246, 2007.

[45] Martin Wainwright, Tommi Jaakkola, and Alan Willsky. Map estimation via agreement on (hyper)trees: Message-passing and linear programming approaches. *IEEE Transactions on Information Theory*, 51:3697–3717, 2002.

[46] J. Yuan, E. Bae, and X.C. Tai. A study on continuous max-flow and min-cut approaches. In *CVPR*, USA, San Francisco, 2010.

[47] Jing Yuan, Egil Bae, Xue-Cheng Tai, and Yuri Boykov. A continuous max-flow approach to potts model. In *ECCV*, 2010.